5-1-2012

Solution to the Electric Field Integral Equation at Arbitrarily Low Frequencies

Jianfang Zhu
Purdue University, zhu3@purdue.edu

Saad Omar
Purdue University, omar0@purdue.edu

Dan Jiao
Purdue University, djiao@purdue.edu

Solution to the Electric Field Integral Equation at Arbitrarily Low Frequencies

Jianfang Zhu

Saad Omar

Dan Jiao

TR-ECE-12-05

May 2, 2012

School of Electrical and Computer Engineering

1285 Electrical Engineering Building

Purdue University

West Lafayette, IN 47907-1285

– This work was supported by a grant from Intel Corporation, a grant from Office of Naval Research under award N00014-10-1-0482, and a grant from NSF under award 0747578.

Solution to the Electric Field Integral Equation at Arbitrarily Low Frequencies

Jianfang Zhu, Saad Omar, and Dan Jiao, *Senior Member, IEEE*

***Abstract*—The low-frequency breakdown problem in electric field integral equation (EFIE) has been well recognized and extensively studied. State of the art methods for solving this problem either reformulate the integral equations or introduce a different set of basis functions. The solution to the original full-wave EFIE with the Rao-Wilton-Glisson (RWG)-basis remains unknown at breakdown frequencies. The contribution of this work is the solution to the original RWG-basis based EFIE at an arbitrarily low frequency including DC. This solution is obtained by deriving a closed-form expression of the inverse of the EFIE system matrix, which is rigorous from high down to any low frequency. We also overcome the low-frequency breakdown caused by the loss of the frequency dependence of the right hand side vector in scattering analysis and the same loss in Green's function in RCS computation. In addition, we develop a fast solution that eliminates the low-frequency breakdown of the EFIE in a reduced system of *O*(1). Instead of introducing additional computational cost to fix the low-frequency breakdown problem, the proposed fast *O*(1) solution speeds up low-frequency computation. Numerical experiments in inductance, capacitance, and RCS extraction at very low frequencies including DC have demonstrated both accuracy and efficiency of the proposed method.**

***Index Terms*— Low-frequency breakdown, electric field integral equation, electromagnetic analysis, scattering, RCS computation, full-wave analysis, fast solution**

I. Introduction

IT has been observed that a full-wave based solution of Maxwell's equations breaks down at low frequencies. Such a problem is especially severe in digital, analog, and mixed-signal integrated circuit applications in which signals have a wide bandwidth from zero to about the third harmonic frequency. In these applications, the breakdown frequency of full-wave solvers is right in the range of circuit operating frequencies.

Existing approaches for overcoming the low-frequency breakdown problem can be categorized into two classes. One class is to stitch a static- or quasi-static based electromagnetic solver with a full-wave based electromagnetic solver. The accuracy of this approach is questionable because static/quasi-static solvers involve fundamental approximations such as decoupled **E** and **H**, which is only true at DC. In addition, at which frequency to switch between different solvers is an issue. In practice, engineers often have to employ an approximation based model to achieve a smooth transition between static, quasi-static, and full-wave solvers, which introduces another level of inaccuracy. Moreover, this approach has an underlying assumption: no frequencies exist at which fullwave solvers break down while the static and/or quasi-static approximations are not valid yet. The validity of this assumption needs to be assessed for different applications.

The other class of methods for solving the low-frequency breakdown problem is to extend the validity of full-wave solvers to low frequencies. In integral equation solvers, these methods include the loop-tree and loop-star basis functions for achieving a natural Helmholtz decomposition of the current at low frequencies, the current-charge integral equation, and the augmented electric field integral equation [1-4]. These methods have successfully extended the validity of full-wave integral equation solvers to much lower frequencies. They have also suggested new research questions to be studied. For example, all of these methods have changed the original system of equations resulting from the traditional method of moments based solution of EFIE with the RWG basis functions. In other words, they switch to a different system of equations to solve Maxwell's equations at low frequencies. The solution to the original RWG-based EFIE, which has been widely used to solve electromagnetic radiation and scattering problems and is theoretically valid from low to high frequencies, remains unknown at low frequencies. There also exist preconditioned EFIE methods for addressing the low-frequency breakdown problem such as Calderón preconditioner based methods [5-8]. However, at low frequencies, the original EFIE-based system matrix, numerically, becomes singular when the contribution from the vector potential is lost due to finite machine precision. No matter how good the preconditioner is, a singular matrix remains singular. To overcome this problem, existing preconditioned EFIE methods still rely on loop-star decomposition, thus again switch to a different system of equations to solve at low frequencies rather than solving the original RWG-based system of equations.

Manuscript received April 18, 2012. This work was supported by a grant from Intel Corporation, a grant from Office of Naval Research under award N00014-10-1-0482, and a grant from NSF under award 0747578.

Jianfang Zhu, Saad Omar, and Dan Jiao are with the School of Electrical and Computer Engineering, Purdue University, 465 Northwestern Avenue, West Lafayette, IN 47907, USA (phone: 765-494-5240; fax: 765-494-3371; e-mail: djiao@purdue.edu).

The contribution of this work is the solution to the original RWG-basis based EFIE at arbitrarily low frequencies including DC. This solution is also rigorous at high frequencies. In the proposed method, we do not change basis functions; we preserve the original EFIE and its system of equations across the whole frequency band. Different from existing methods that tackle the low-frequency breakdown from the perspective of how to change the original matrix, we derive a closed-form expression of the inverse of the EFIE system matrix at any frequency. By doing so, we bypass the barrier of finite machine precision and avoid the breakdown caused by numerically solving the original system matrix. The closed-form expression of the inverse of the EFIE system matrix is rigorously derived from the eigenvectors and eigenvalues of a generalized eigenvalue problem governing the EFIE-based numerical system. Different from the same eigenvalue problem governing a finite-element based numerical system [9-10], which is frequency independent, the generalized eigenvalue problem governing the EFIE is frequency dependent because of Green's function. However, this frequency-dependent generalized eigenvalue problem can still be solved at an arbitrarily low frequency without breakdown. In fact, at very low frequencies including DC, this generalized eigenvalue problem becomes frequency independent. With the proposed closed-form expression of the inverse, the frequency dependence of the EFIE solution is explicitly revealed from high frequencies down to low frequencies. From this inverse model, the solution to the EFIE can be found at an arbitrarily low frequency including zero frequency.

Interestingly, in this work, in addition to the breakdown caused by the loss of the vector potential in the EFIE system matrix, we have also found the breakdown due to the loss of the frequency dependence of the right hand side vector in scattering analysis, as well as the breakdown caused by the loss of the frequency dependence of Green's function in scattered field computation. These two problems have been identified before [1, 11-12] and termed as numerical cancellation problems. In the context of the proposed work, the frequency dependence of the right hand side vector is lost at low frequencies when performing the inner product between the divergence-free component of the EFIE solution with the incident field. Similarly, the frequency dependence of Green's function is lost at low frequencies when performing the inner product between the divergence-free current with Green's function to evaluate the scattered field. The two problems are readily fixed in this work by removing the gradient-field component of the incident field and Green's function when computing their inner products with a divergence-free current since the inner product between a divergence-free current and a gradient field is analytically known to be zero.

Moreover, the proposed theoretical model of the EFIE's inverse and EFIE's solution suggests that one can use one solution vector obtained from the traditional EFIE solver to reduce the original EFIE system of $O(N)$ to a system of $O(1)$, and then fix the low-frequency breakdown problem in the reduced $O(1)$ system. In this way, we equally bypass the barrier of finite machine precision; preserve the theoretical rigor of the proposed solution, while obtaining the EFIE solution at low frequencies including DC without introducing additional computational cost. Instead, we accelerate the low-frequency computation by obtaining the EFIE solution in $O(1)$ complexity.

The remaining of this paper is organized as follows. In Section II, we give a brief overview of the low frequency breakdown problem of the EFIE. In Section III, we present the solution to the original RWG-basis based EFIE at any low frequency. In Section IV, we present a fast $O(1)$ method. In Section V, we simulate a number of circuit and scattering examples having a very small electric size including zero to demonstrate the accuracy and efficiency of the proposed solution. Section VI relates to our conclusion.

II. THE LOW-FREQUENCY BREAKDOWN PROBLEM OF EFIE

A. MoM Solution of EFIE

Consider a perfect electrically conducting object immersed in a medium with permittivity ε and permeability μ. The object is excited by an impressed source $\mathbf{E}_i$ that induces current $\mathbf{J}$ on the conducting surface. The source $\mathbf{E}_i$ can be a delta-gap voltage source commonly used for analyzing radiation and circuit problems; it can also be an incident field employed for scattering analysis. The current $\mathbf{J}$ satisfies the following electric field integral equation:

$$\hat{n}\times\mathbf{E}_i = \hat{n}\times\{\iint_S [j\omega\mu\mathbf{J}(\mathbf{r}')G(\mathbf{r},\mathbf{r}') + \frac{1}{j\omega\varepsilon}(\nabla'\bullet\mathbf{J}(\mathbf{r}')\nabla' G(\mathbf{r},\mathbf{r}')]dS\}\ , \quad (1)$$

in which $\mathbf{r}$ and $\mathbf{r}$' are, respectively, observation and source points on the conducting surface, $\hat{n}$ is a unit vector normal to conducting surface, and G is dynamic Green's function

$$G(\mathbf{r},\mathbf{r}') = \frac{e^{-jk|\mathbf{r}-\mathbf{r}'|}}{4\pi|\mathbf{r}-\mathbf{r}'|}\ , \quad (2)$$

where k is wave number $\omega\sqrt{\mu\varepsilon}$, and ω is angular frequency.

By expanding the unknown surface current density $\mathbf{J}$ using RWG basis functions [13], and applying Galerkin's method to (1), we obtain the following linear system of equations

$$\mathbf{Z}(\omega)\ I(\omega) = V(\omega)\,, \quad (3)$$

where system matrix $\mathbf{Z}$ is

$$\mathbf{Z}(\omega)\ = \frac{1}{j\omega}\mathbf{\Phi}(\omega) + j\omega\mathbf{A}(\omega)\ , \quad (4)$$

in which $\mathbf{A}$ and $\mathbf{\Phi}$ are frequency dependent, the elements of which are given by

$$\mathbf{A}_{mn} = \iint_{S_m} dS \iint_{S_n} [\mu\mathbf{J}_m(\mathbf{r})\cdot\mathbf{J}_n(\mathbf{r}')G(\mathbf{r},\mathbf{r}')]dS' \quad (5)$$

$$\mathbf{\Phi}_{mn} = \iint_{S_m} dS \iint_{S_n} [\frac{1}{\varepsilon}\nabla\bullet\mathbf{J}_m(\mathbf{r})\nabla'\bullet\mathbf{J}_n(\mathbf{r}')G(\mathbf{r},\mathbf{r}')]dS'\ , \quad (6)$$

with $\mathbf{J}_m$ ($\mathbf{J}_n$) being the vector basis used to expand unknown current $\mathbf{J}$. The right hand side of (3) has the following entries:

$$V_m = \iint_{S_m} \mathbf{J}_m(\mathbf{r}) \cdot \mathbf{E}_i(\mathbf{r}) dS \cdot \quad (7)$$

As can be seen from (4), matrix **Z** is composed of two matrices **Φ** and **A**, each of which is associated with a different frequency dependence. A careful examination of the matrix properties of **Φ** and **A** reveals that **A** is a full-rank matrix while **Φ** is rank deficient. The deficiency of **Φ** is due to the nullspace of the divergence operator. Specifically, any solenoidal vector **J** satisfying $\nabla \bullet \mathbf{J} = 0$ would satisfy $\mathbf{\Phi} J = 0$. Therefore, **Φ** is a singular matrix.

B. Analysis of the Low-Frequency Breakdown Problem

To analyze the low-frequency breakdown problem, we examine the ratio of **A**'s norm over **Φ**'s norm. It is proportional to l^2/c^2, where c is the speed of light, and l is the smallest mesh size. As an example, for state-of-the-art integrated circuits with μm-level geometrical dimensions, this ratio is in the order of 10^{-30}. Consequently, at and below tens of MHz, $\omega^2\mathbf{A}$ is sixteen orders of magnitude smaller than **Φ**. Even one uses double-precision computing, **A** is essentially treated as zero by computers when performing the addition of $j\omega\mathbf{A}$ and $\mathbf{\Phi}/(j\omega)$ in (4). As a result, the solution of (3) breaks down. It should also be noted that the ratio of $\omega^2\mathbf{A}$'s norm over **Φ**'s norm is proportional to the square of the electric size. As a result, the frequency at which the EFIE breaks down is different for different feature sizes. For integrated circuits with μm-level dimensions, the breakdown frequency is in the range of MHz, which is right in the circuit operating frequencies, and hence becoming a great concern. In contrast, for traditional full-wave applications such as antennas and microwave circuits, although the EFIE also breaks down at low frequencies, the breakdown frequency is much lower than the typical operating frequencies of the microwave circuits and antennas, and hence the low-frequency breakdown of EFIE has not become a great concern in those areas although the breakdown problem also exists.

As can be seen from the aforementioned analysis, the root cause of the low-frequency breakdown is finite machine precision, which has been recognized by many early papers in this area [1-4]. Computers always have a finite precision. Apparently, changing the system matrix (4) to a different one that is solvable at low frequencies seems to be the only way forward. However, by doing so, we incur additional computational cost. In addition, we need to determine at which frequency to switch to a new formulation. We also need to assess the accuracy of the new formulation at different frequencies. More important, since the ratio of $\omega^2\mathbf{A}$'s norm over **Φ**'s norm is proportional to the square of the electric size of the *smallest feature size* of the problem being simulated, at the breakdown frequency, it is possible that the *largest size* of the problem is not small compared to wavelength when simulating a multiscale problem spanning many orders of magnitude difference in geometrical scales. Hence, there exists a possibility that when the EFIE solution breaks down, the solution is still dominated by full-wave physics. In view of this, it is necessary to find the solution of (4) as it is at any breakdown frequency.

III. PROPOSED SOLUTION

In the study of the low-frequency breakdown of EFIE, we found that one can encounter three breakdown phenomena. If any of the three breakdown problems is not solved, the EFIE breakdown cannot be completely solved. The first breakdown is due to the loss of the vector potential term in the EFIE system matrix at low frequencies; the second breakdown is caused by the loss of the frequency dependence of the right hand side vector such as a plane wave incidence used in scattering analysis; and the third breakdown occurs when evaluating the scattered field generated by the divergence-free component of the current. In the following three subsections, we show how each breakdown is overcome in this work.

A. Analytical Derivation of the Inverse of the EFIE-Based System Matrix

The solution of (3) resulting from the discretization of EFIE is governed by the following generalized eigenvalue problem

$$\mathbf{\Phi}(\omega)x = \lambda \mathbf{A}(\omega)x \ , \quad (8)$$

where **Φ** and **A** are the same as those in (4), λ is the eigenvalue, and x is the corresponding eigenvector. Since $\mathbf{A}$ is symmetric definite and **Φ** is symmetric indefinite, the eigenvalues λ are finite numbers, including zeros due to the nullspace of **Φ**. Meanwhile, the eigenvectors x are linearly independent of each other [14]. Different from the system matrices resulting from a finite element based analysis, due to Green's function, **Φ** and **A** are both complex valued and frequency dependent. Therefore, the generalized eigenvalue problem shown in (8) is frequency dependent. Only at low frequencies where $e^{-jk|\mathbf{r}-\mathbf{r}'|}$ in (2) can be approximated as 1, **Φ** and **A** can be considered real, and (8) becomes frequency independent.

Denoting the eigenvalues of (8) by $\lambda_1, \lambda_2, \ldots, \lambda_N$ and the corresponding eigenvectors by $x_1, x_2, \ldots, x_N$. Let **W** be the matrix whose column vectors are eigenvectors

$$\mathbf{W} = [x_1, x_2, \cdots, x_N], \quad (9)$$

and Λ be the diagonal matrix of eigenvalues

$$\Lambda = \begin{bmatrix} \lambda_1 & & \\ & \ddots & \\ & & \lambda_N \end{bmatrix}. \quad (10)$$

Since **W** is full rank, its column vectors constitute a complete set of bases in an N dimensional space. Thus, we can use **W** to expand the unknown current vector I in (3). We thereby obtain

$$I = \mathbf{W}\tilde{I} \ , \quad (11)$$

in which $\tilde{I}$ is the unknown coefficient vector to be solved. Substituting (11) into (3), and multiplying (3) by $\mathbf{W}^T$ on both sides, we obtain

$$(\frac{1}{j\omega}\tilde{\mathbf{\Phi}} + j\omega\tilde{\mathbf{A}})\tilde{I} = \tilde{V} \ , \quad (12)$$

where

$$\tilde{\mathbf{\Phi}} = \mathbf{W}^T\mathbf{\Phi}\mathbf{W}, \ \tilde{\mathbf{A}} = \mathbf{W}^T\mathbf{A}\mathbf{W} \quad (13)$$

$$\tilde{V} = \mathbf{W}^T V \,. \tag{14}$$

Since $\mathbf{W}$ is the eigenvector matrix, and Λ is the eigenvalue matrix, from (8), we have

$$\mathbf{\Phi W} = \mathbf{AW\Lambda} \,. \tag{15}$$

Multiplying both sides by $\mathbf{W^T}$, we obtain

$$\mathbf{W}^T\mathbf{\Phi W} = \mathbf{W}^T\mathbf{AW\Lambda} \,, \tag{16}$$

from which and (13), we find

$$\tilde{\mathbf{\Phi}} = \tilde{\mathbf{A}}\mathbf{\Lambda} \,. \tag{17}$$

Substituting (17) into (12), we have

$$\begin{pmatrix} \dfrac{\lambda_1 - \omega^2}{j\omega} & & \\ & \ddots & \\ & & \dfrac{\lambda_N - \omega^2}{j\omega} \end{pmatrix} \tilde{I} = \tilde{\mathbf{A}}^{-1}\tilde{V} \,. \tag{18}$$

Thus, the unknown coefficient vector $\tilde{I}$ can be found by solving a diagonal system (18), from which the original solution I can be obtained using (11).

The above derivation is for one right hand side V in (3). If the right hand side V is an identity matrix, we obtain the inverse of $\mathbf{Z}$ at an arbitrary ω, which is:

$$\mathbf{Z}(\omega)^{-1} = j\omega\mathbf{W}(\mathbf{\Lambda} - \omega^2\mathbf{I})^{-1}(\mathbf{W}^T\mathbf{AW})^{-1}\mathbf{W}^T, \ \forall\omega \tag{19}$$

where $\mathbf{I}$ is an identity matrix.

At low frequencies where $\mathbf{A}$ and $\mathbf{\Phi}$ become real, $\mathbf{A}$ is positive definite, $\mathbf{\Phi}$ is semi-positive definite. The (8) is said to be a symmetric positive definite generalized eigenvalue problem [15]. For this class of problem, the eigenvectors are both $\mathbf{\Phi}$- and $\mathbf{A}$-orthogonal. Hence, we have

$$\begin{aligned} &\mathbf{W}^T\mathbf{AW} = \mathbf{I}, \ \mathbf{W}^T\mathbf{\Phi W} = \mathbf{\Lambda}, \\ &\omega \in \{\omega \text{ at which } e^{-jk|\mathbf{r}-\mathbf{r}'|} \sim 1\} \end{aligned} \tag{20}$$

Thus, (19) becomes

$$\mathbf{Z}(\omega)^{-1} = j\omega\mathbf{W}(\mathbf{\Lambda} - \omega^2\mathbf{I})^{-1}\mathbf{W}^T \,. \tag{21}$$

In the above, by analytically deriving the inverse of the EFIE-based system matrix $\mathbf{Z}$, we avoid the breakdown caused by the loss of the vector potential term when numerically solving $\mathbf{Z}$. However, the inverse shown in (19) and (21) can still break down at low frequencies if the inexact zero eigenvalues of (8) are not fixed to be exact zero. The details are given below.

The eigenvalues of (8) can be divided into two groups: one group is associated with the nullspace of $\mathbf{\Phi}$, and the other is associated with the nonzero resonance frequencies of the structure. The first group has zero eigenvalues. But numerically, they cannot be computed as exact zeros. Instead, they can be compued as very large numbers. For example, in a typical on-chip circuit having μm-level dimensions, the largest eigenvalue of (8) can be as large as 10^{32} while the zero eigenvalues are numerically obtained as 10^{16}. This is because eigenvalue solvers first converge to the largest eigenvalue of the numerical system in general, the eigenvalues that are sixteen orders of magnitude smaller than the largest one are not distinguishable in double-precision computing. Even though these inexact zero eigenvalues do not induce much error at high frequencies, they lead to a completely wrong frequency dependence of the EFIE solution at low frequencies. To expain, as can be seen from (18), for a low ω, if the zero eigenvalues are computed to be a nonzero value, when ω is comparable to the nonzero value, the resultant $\tilde{I}$ can become totally wrong. For example, λ_1 is analytically known to be zero but computed as a nonzero value a. The corresponding entry $\tilde{I}_1$ becomes proportional to $\dfrac{j\omega}{a-\omega^2}$, whereas the right $\tilde{I}_1$ should scale with frequency as $\dfrac{j\omega}{-\omega^2}$, and hence $\dfrac{1}{j\omega}$. This error is negligible at high frequencies since a compared to a high ω^2 is negligible. However, at low frequencies, this error leads to a completely wrong frequency dependence. A natural remedy to the inexact zero eigenvalue problem is to fix the inexact zero eigenvalues to be exact zeros. Since in magnitude, zero eigenvalues are the smallest eigenvalues of (8) and there is a clear gap between the first nonzero eigenvalue and the zero eigenvalue as the structure being simulated is finite, the zero eigenvalues can be readily identified and their inaccuracy can be analytically fixed.

With the inexact zero eigenvalues fixed to be exact zeros, (19) becomes

$$\mathbf{Z}(\omega)^{-1} = j\omega(\mathbf{W}_0 \ \mathbf{W}_h)\begin{bmatrix} 0-\omega^2\mathbf{I} & 0 \\ 0 & \Lambda_h - \omega^2\mathbf{I} \end{bmatrix}^{-1}(\mathbf{W}^T\mathbf{AW})^{-1}\mathbf{W}^T, \ \forall\omega \tag{22}$$

where $\mathbf{W}_0$ and $\mathbf{W}_h$, respectively, represent the eigenvectors of (8) corresponding to zero and nonzero eigenvalues; $\mathbf{W}$ is the union of $\mathbf{W}_0$ and $\mathbf{W}_h$, i.e. $\mathbf{W} = [\mathbf{W}_0 \ \mathbf{W}_h]$; and Λ_h is the diagonal matrix of nonzero eigenvalues. The $\mathbf{W}_0$ is clearly the nullspace of $\mathbf{\Phi}$ since it satisfies

$$\mathbf{\Phi W}_0 = 0 \,. \tag{23}$$

In what follows, for convenience, we call $\mathbf{W}_0$ DC eigenmodes while $\mathbf{W}_h$ higher-order eigenmodes since the former corresponds to a zero resonance frequency, whereas the latter has a higher resonance frequency.

The inverse of the EFIE-based system matrix derived in (22) is true from high frequencies down to any low frequency. It does not suffer from low-frequency breakdown. This is because given an arbitrary frequency ω, $\mathbf{W}_0$, $\mathbf{W}_h$, and Λ_h in (22) can be accurately found from (8) without breakdown. Since $\mathbf{W}$ is full rank and $\mathbf{A}$ is invertible, $(\mathbf{W}^T\mathbf{AW})^{-1}$ in (22) can also be obtained at any frequency. At zero frequency, both $\mathbf{\Phi}$ and $\mathbf{A}$ become real. In addition, $\mathbf{\Phi}$ is semi-positive definite and $\mathbf{A}$ is positive definite, which render the eigenvalues of (8) non-negative and real, and $\mathbf{W}^T\mathbf{AW} = \mathbf{I}$ as shown in (20). As a result, using (22), we can obtain a correct inverse at an arbitrarily low frequency including DC. Moroever, (22) is rigorous at high frequencies also.

At low frequencies where $\mathbf{A}$ and $\mathbf{\Phi}$ become real, (8) and hence $\mathbf{W}_0$ and $\mathbf{W}_h$ become frequency independent. In this case, due to (20), (22) can be written as

$$\mathbf{Z}(\omega)^{-1} = j\omega(\mathbf{W}_0\ \mathbf{W}_h)\begin{bmatrix}0-\omega^2\mathbf{I} & 0\\ 0 & \Lambda_h-\omega^2\mathbf{I}\end{bmatrix}^{-1}(\mathbf{W}_0\ \mathbf{W}_h)^T = \frac{1}{j\omega}\mathbf{W}_0\mathbf{W}_0{}^T + j\omega\mathbf{W}_h(\Lambda_h-\omega^2\mathbf{I})^{-1}\mathbf{W}_h{}^T \quad (24)$$

which can be further reduced to

$$\mathbf{Z}(\omega)^{-1} = \frac{1}{j\omega}\mathbf{W}_0\mathbf{W}_0{}^T + j\omega\mathbf{W}_h(\Lambda_h)^{-1}\mathbf{W}_h{}^T \quad (25)$$

when ω^2 compared to Λ_h is negligible.

B. Solution to the EFIE at an Arbitrary Frequency

Based on (22), the solution of (3) at an arbitrary ω can be written as

$$I(\omega) = \mathbf{Z}(\omega)^{-1}V = j\omega(\mathbf{W}_0\ \mathbf{W}_h)\begin{bmatrix}0-\omega^2\mathbf{I} & 0\\ 0 & \Lambda_h-\omega^2\mathbf{I}\end{bmatrix}^{-1}(\mathbf{W}^T\mathbf{A}\mathbf{W})^{-1}\mathbf{W}^TV = I_0 + I_h \quad (\forall\omega) \quad (26)$$

where I_0 represents the contribution from all the DC eigenmodes

$$I_0 = \frac{1}{j\omega}\mathbf{W}_0\left\{(\mathbf{W}^T\mathbf{A}\mathbf{W})^{-1}\mathbf{W}^TV\right\}_0, \quad (27)$$

which is a divergence-free current since $\mathbf{W}_0$ is the nullspace of $\mathbf{\Phi}$, and I_h represents the contribution from all the higher-order eigenmodes

$$I_h = j\omega\mathbf{W}_h\left(\Lambda_h-\omega^2\mathbf{I}\right)^{-1}\left\{(\mathbf{W}^T\mathbf{A}\mathbf{W})^{-1}\mathbf{W}^TV\right\}_h. \quad (28)$$

In (27), $\left\{(\mathbf{W}^T\mathbf{A}\mathbf{W})^{-1}\mathbf{W}^TV\right\}_0$ denotes the part of vector $\{(\mathbf{W}^T\mathbf{A}\mathbf{W})^{-1}\mathbf{W}^TV\}$ scaled by $\frac{-1}{\omega^2}$ and then multipled by $\mathbf{W}_0$, and $\left\{(\mathbf{W}^T\mathbf{A}\mathbf{W})^{-1}\mathbf{W}^TV\right\}_h$ in (28) is the remainging part of $\{(\mathbf{W}^T\mathbf{A}\mathbf{W})^{-1}\mathbf{W}^TV\}$.

The EFIE solution (26) is true at both high and low frequencies. At low frequencies where $\mathbf{A}$ and $\mathbf{\Phi}$ become real, from (24), we obtain

$$I_0 = \frac{1}{j\omega}\mathbf{W}_0\mathbf{W}_0{}^TV \quad (29)$$

and

$$I_h = j\omega\mathbf{W}_h\left(\Lambda_h-\omega^2\right)^{-1}\mathbf{W}_h{}^TV. \quad (30)$$

The right hand side vector V in (29) and (30) can be either frequency independent or frequency dependent. The former is generally used for circuit and antenna analysis; while the latter is often encountered in scattering analysis when an incident plane wave is used as the excitation. When V is frequency dependent, if it is not handled correctly, even though the inverse of the EFIE system matrix is obtained rigorously at low frequencies, the solution of EFIE can still break down, the detail of which is given in the following subsection.

B.1 Solution to the frequency-dependent right hand side V encountered in scattering analysis

In scattering analysis, V in (3) represents an incident plane wave. It is frequency dependent. However, at low frequencies, it becomes a constant in computer simulation when the phase of the plane wave is too small to be captured by finite machine precision. As a result, the I_0 shown in (29), which is the divergence-free current, becomes inversely proportional to frequency. This frequency dependence is wrong since at low frequencies, theoretically speaking, the divergence-free current is induced by incident magnetic field, which should become a constant at low frequencies. To solve such a breakdown problem originated from the right hand side of the EFIE system, we develop the following method.

The incident plane wave can be written as

$$\mathbf{E}_i(\omega) = -\nabla\varphi - j\omega\mathbf{A}, \quad (31)$$

where both scalar potential φ and vector potential $\mathbf{A}$ terms exist as long as frequency is not zero. With (31), the $\mathbf{W}_0{}^TV$ in (29) can be written as

$$\mathbf{W}_0{}^TV = \mathbf{W}_0{}^T(V_{\nabla\varphi} + j\omega V_{\mathbf{A}}), \quad (32)$$

in which is $V_{\nabla\varphi}$ is V corresponding to the $\nabla\varphi$ component of the incident field, and $V_{\mathbf{A}}$ is V corresponding to the $\mathbf{A}$-component of the incident field. Since $\mathbf{W}_0$ represents a divergence-free current, which can be written as $\nabla\times(\psi\hat{n})$ and hence $\hat{n}\times\nabla\psi$ [11] with ψ being a scalar, its inner product with a gradient field can be analytically proved to be zero. As a result, (32) becomes

$$\mathbf{W}_0{}^TV = \mathbf{W}_0{}^T(j\omega V_{\mathbf{A}}). \quad (33)$$

If we do not utilize the analytical property of $\mathbf{W}_0{}^TV_{\nabla\varphi} = 0$ to vanish the $V_{\nabla\varphi}$ term in (32), at low frequencies where $j\omega V_{\mathbf{A}}$ is negligible, (32) will be dominated by $\mathbf{W}_0{}^TV_{\nabla\varphi}$. Thus the $\mathbf{W}_0{}^TV$ will have a completely wrong frequency dependence at low frequencies.

With (33), (29) becomes

$$I_0 = \frac{1}{j\omega}\mathbf{W}_0\mathbf{W}_0{}^T(j\omega V_{\mathbf{A}}) = \mathbf{W}_0\mathbf{W}_0{}^TV_{\mathbf{A}}. \quad (34)$$

Hence, at very low frequencies, the divergence-free current I_0 for a plane wave excitation is a constant that does not change with frequency, which agrees with low-frequency electromagnetic field theory [16]. As for the nonsolenoidal component of the current, from (30), we obtain

$$I_h = j\omega\mathbf{W}_h\left(\Lambda_h\right)^{-1}\mathbf{W}_h{}^TV \quad (35)$$

at low frequencies, which also agrees with the low-frequency electromagnetics as it represents the current associated with a charge having a constant magnitude, and hence scaling with frequency linearly.

The $j\omega V_{\mathbf{A}}$ in (34) can be readily obtained by setting the incident field as

$$\mathbf{E}_i(\omega) = \mathbf{E}_i(\omega) - \mathbf{E}_i(\omega=0)$$

when evaluating (7), i.e. $j\omega V_{\mathbf{A}}$ can be computed by

$$j\omega V_{\mathbf{A},m} = \iint_{S_m}\mathbf{J}_m(\mathbf{r})\cdot\left[\mathbf{E}_i(\omega)-\mathbf{E}_i(\omega=0)\right]dS, \quad (36)$$

where $\mathbf{E}_i(\omega=0)$ is the incident field at zero frequency, which is nothing but the gradient-field component of the incident field as can be seen clearly from (31).

In summary, to avoid the breakdown caused by the frequency-dependent right hand side V, we analytically vanish the gradient-field component of V when evaluating $\mathbf{W}_0^T V$, i.e. the inner product between the divergence-free current and the right hand side vector. Since the inner product between a divergence-free current and a gradient field is zero irrespective of frequency, such a treatment is universal across all frequencies. Hence, in (26), (27) and (28) that are true for all frequencies, the $\mathbf{W}_0^T V$ term can be corrected in the same way. As for the evaluation of $\mathbf{W}_h^T V$, it can be evaluated as it is without suffering from the low-frequency breakdown.

B.2 Solution to the frequency- independent right hand side V

In many applications such as circuit extraction and antenna impedance calculation, the right hand side V used is frequency independent. In this case, the frequency dependence of I_0 and I_h can be straightforwardly recognized from (29) and (30). In addition, the weights of the higher-order eigenmodes in the current solution are proportional to $j\omega\left(\Lambda_h-\omega^2\right)^{-1}$, whereas that of the DC eigenmodes scale as $1/\omega$. At low frequencies where the former becomes negligible, the EFIE solution becomes I_0, thus the divergence-free current. Therefore, the impedance of the structure being simulated is proportional to $j\omega$, which agrees with the physical understanding that for a constant voltage excitation, a perfect conductor structure behaves as an ideal inductor at low frequencies. In addition, at zero frequency, it is a short circuit having zero impedance, yielding an infinite current for a constant voltage excitation, which agress with the result shown in (29).

C. RCS Computation from Zero to High Frequencies

The computation of RCS also breaks down at low frequencies if not done correctly. In this section, we give a detailed formula for evaluating RCS from high down to any low frequency.

The RCS is defined as

$$\mathrm{RCS}=\lim_{r\to\infty}4\pi r^2\frac{|\mathbf{E}^{sca}(\mathbf{r})|^2}{|\mathbf{E}^{inc}|^2}, \tag{37}$$

where the scattered $\mathbf{E}$ field, $\mathbf{E}^{sca}(\mathbf{r})$, can be computed from the current $\mathbf{J}$ as the following

$$\mathbf{E}^{sca}(\mathbf{r})=\iint_S[j\omega\mu\mathbf{J}(\mathbf{r}')G(\mathbf{r},\mathbf{r}')+\frac{1}{j\omega\varepsilon}(\nabla\bullet\mathbf{J}(\mathbf{r}')\nabla G(\mathbf{r},\mathbf{r}')]dS \tag{38}$$

In far field analysis, we consider θ- and φ-component of the $\mathbf{E}^{sca}(\mathbf{r})$, which is only contributed by the first component of (38). This component is associated with the vector potential. It can be evaluated as

$$\lim_{r\to\infty}\iint_S[j\omega\mu\mathbf{J}(\mathbf{r}')G(\mathbf{r},\mathbf{r}')=\frac{j\omega\mu}{4\pi r}e^{-jkr}\iint_S\mathbf{J}(\mathbf{r}')e^{jkr'\cos\psi}dS, \tag{39}$$

where

$$\cos\psi=\frac{\mathbf{r}\cdot\mathbf{r}'}{rr'}. \tag{40}$$

From (26-28), it can be seen that at any frequency that is either high or low, current $\mathbf{J}$ can be written as

$$\mathbf{J}=\tilde{\mathbf{J}}_0(\omega)+\tilde{\mathbf{J}}_h(\omega), \tag{41}$$

where $\tilde{\mathbf{J}}_0$ is the divergence-free current associated with $\mathbf{W}_0$, and $\tilde{\mathbf{J}}_h$ is the nonsolenoidal current associated with $\mathbf{W}_h$.

By subsitituting (41) into (39), we obtain

$$\lim_{r\to\infty}\iint_S[j\omega\mu\mathbf{J}(\mathbf{r}')G(\mathbf{r},\mathbf{r}')=$$
$$=\frac{j\omega\mu}{4\pi r}e^{-jkr}\iint_S\tilde{\mathbf{J}}_0e^{jkr'\cos\psi}dS+\frac{j\omega\mu}{4\pi r}e^{-jkr}\iint_S\tilde{\mathbf{J}}_he^{jkr'\cos\psi}dS \tag{42}$$

In the above, the computation of the first term breaks down at low frequencies. This is because the correct frequency-dependence of the first term will be lost when $e^{jkr'\cos\psi}$ is treated as 1 in computation at low frequencies. To fix this problem, again, like the approach we develop to fix the low-frequency breakdown of $\mathbf{W}_0^T V$ in Section III.B, we split $e^{jkr'\cos\psi}$ into a gradient-field component and a component associated with vector potential. (Notice that although $e^{jkr'\cos\psi}$ is a scalar, we need to take the dot product of $\tilde{\mathbf{J}}_0$ with $e^{jkr'\cos\psi}\hat{\theta}$ and $e^{jkr'\cos\psi}\hat{\varphi}$ to respectively obtain the θ- and φ-component of the scattered field generated by the divergence-free current $\tilde{\mathbf{J}}_0$.) We then analytically vanish the gradient-field related component of $e^{jkr'\cos\psi}$ because the inner product of the divergence-free current $\tilde{\mathbf{J}}_0$ and a gradient field is analytically known to be zero. Thus, (42) is corrected to be

$$\lim_{r\to\infty}\iint_S[j\omega\mu\mathbf{J}(\mathbf{r}')G(\mathbf{r},\mathbf{r}')=$$
$$=\frac{j\omega\mu}{4\pi r}e^{-jkr}\iint_S\tilde{\mathbf{J}}_0(e^{jkr'\cos\psi}-1)dS+\frac{j\omega\mu}{4\pi r}e^{-jkr}\iint_S\tilde{\mathbf{J}}_he^{jkr'\cos\psi}dS, \tag{43}$$

where 1 is nothing but the gradient-field component of $e^{jkr'\cos\psi}$. As a result, the low-frequency breakdown of the first-term in (42) is fixed. Moreover, (43) is true at high frequencies also. Thus, one can use it to obtain correct RCS at any frequency. The $\tilde{\mathbf{J}}_0$ and $\tilde{\mathbf{J}}_h$ in (43) can be evaluated respectively from (27) and (28), with $\mathbf{W}_0^T V$ in which evaluated based on (33), without making any approximation.

From (43), we can also analyze the frequency dependence of $\mathbf{E}^{sca}(\mathbf{r})$ at low frequencies. Since at low frequencies, $\tilde{\mathbf{J}}_0$ is a constant as can be seen from (34), while $\tilde{\mathbf{J}}_h$ scales linearly with frequency as shown in (35), both terms in (43) scale with frequency quadratically. In other words, the scattered field generated by both the divergence-free current and the nonsolenoidal current scales quadratially with frequency at

low frequencies, and at DC, the scattered field in the far field is zero.

IV. PROPOSED FAST $O(1)$ SOLUTION

With the true solution of the original EFIE found at any low frequency in Section III, we can develop a fast method to speed up the EFIE computation at low frequencies where the traditional solution breaks down. Instead of introducing additional computational cost to fix the low-frequency breakdown, this fast method accelerates the low-frequency computation with its $O(1)$ solution. The detail of this method is given below.

For a frequency-independent right hand side V, from (29) and (30), it is clear that at low frequencies, the current solution is purely imaginary. When the contribution from higher-order eigenmodes, (30), is negligible, the space where the EFIE solution resides is $\mathbf{W}_0$ as shown by (29). $\mathbf{W}_0$ is the nullspace of $\mathbf{\Phi}$. The dimension of $\mathbf{\Phi}$'s nullspace can be large and, also, grows with matrix size linearly. However, the nullspace vectors share the same zero eigenvalue in common although they are linearly independent of each other. Based on this fact, we can use the right hand side vector to shrink the dimension of this space to 1. To explain, given a right hand side of (3), V, the contributions from all the nullspace vectors in the EFIE solution are, in fact, grouped together and can be represented by a single vector w_0 as shown below:

$$I(\omega) = \frac{1}{j\omega}\mathbf{W}_0\mathbf{W}_0{}^T V = \frac{1}{j\omega} w_0 \ . \tag{44}$$

A grouping like (44) would not be possible if the eigenvectors in $\mathbf{W}_0$ do not share the same eigenvalue in common.

What is implied by (44) is significant: given a right hand side, one vector is adequate to span the low frequency solution of the EFIE. Hence, as long as we can find the single vector w_0, given a frequency regardless of how low it is, we can expand the field solution in this $O(1)$ space, and transform the original system of $O(N)$ shown in (3) to an $O(1)$ system, from which the low-frequency breakdown problem can be readily fixed.

To obtain w_0 and also avoid solving the generalized eigenvalue problem shown in (8), we develop the following approach. As can be seen from (29) and (30), at a low frequency where the contribution from higher-order eigenmodes I_h is negligible, the current solution $I(\omega)$ is in the space formed by a single vector w_0. Therefore, we can use one solution vector obtained at such a frequency as a complete and accurate representation of the space formed by w_0. Denoting such a frequency by ω_{ref}, we solve the original system (3) as it is and obtain a single solution vector, which is denoted by I_{ref}. With I_{ref}, given any low frequency ω, we can expand the solution of the EFIE system (3) by using

$$I(\omega) = I_{ref} y \,, \tag{45}$$

with unknown coefficient y solved as the following:

$$I_{ref}^T(\mathbf{\Phi}(\omega) - \omega^2\mathbf{A}(\omega))I_{ref} y = I_{ref}^T V(\omega) \,. \tag{46}$$

As a result, the system is reduced to a one by one system. However, the low frequency breakdown problem still remains in the reduced $O(1)$ system when the term associated with ω^2 is neglected due to finite machine precision. This can be readily fixed by recognizing that w_0 is in the nullspace of $\mathbf{\Phi}$, and hence $\mathbf{\Phi} I_{ref} = 0$. Thus (46) becomes:

$$I_{ref}^T(\omega^2\mathbf{A}(\omega))I_{ref} y = I_{ref}^T V(\omega) \tag{47}$$

which can be solved at any low frequency without breakdown. With unknown coefficient y solved from (47), the current solution can be recovered from (45). In this way, we can rapidly fix the low frequency breakdown problem, and meanwhile retaining the theoretical rigor of the EFIE solution derived in Section III.

The remaining question is how to choose ω_{ref}. From (29) and (30), the weight of a higher-order mode having eigenvalue λ_h in the EFIE solution is proportional to $\omega/(\lambda_h - \omega^2)$; the weight of the DC mode in the EFIE solution is proportional to $1/\omega$. The former over the latter is $\frac{1}{\lambda_h/\omega^2 - 1}$. Therefore $\omega_{ref}{}^2$ can be chosen as the following

$$\omega_{break}{}^2 < \omega_{ref}{}^2 < 10^{-p}\lambda_{h1} \tag{48}$$

where $p \geq 2$, ω_{break} is the breakdown frequency, and λ_{h1} is the first nonzero eigenvalue of (8). At such a $\omega_{ref}{}^2$, the weight of the higher-order mode is at least two orders of magnitude smaller than that of the DC eigenmode, and thereby negligible. In double precision computing, the ω_{break} can be determined based on

$$\omega^2_{break} \leq 10^{-16}\frac{\|\mathbf{\Phi}\|}{\|\mathbf{A}\|} \,. \tag{49}$$

This is because as analyzed in Section II.B, when the solution of (3) breaks down, in double precision computing, the norm of $\omega^2\mathbf{A}$ is sixteen orders of magnitude smaller than that of $\mathbf{\Phi}$. The λ_{h1} (having the same unit as ω^2) can be analytically estimated from the first nonzero resonance frequency of the structure being simulated, which corresponds to the largest physical dimension of the structure.

It is worth mentioning that in (48), $10^{-p}\lambda_{h1} > \omega_{break}{}^2$ ($p \geq 2$) is, in general, satisfied for practical applications. This is because the difference between $\omega_{break}{}^2$ and the largest eigenvalue of (8) is beyond machine precision (that is why the EFIE solution breaks down), while the difference between λ_{h1} (smallest nonzero eigenvalue) and the largest eigenvalue is within machine precision and less than 14 orders of magnitude difference in general. It is possible that in future applications where the difference between λ_{h1} and the largest eigenvalue is pushed close to machine precision such as a multiscale application that covers many orders of magnitude difference in geometrical scales, then when theEFIE solution breaks down, not only DC eigenmodes, but also nonzero higher-order eigenmodes can contribute to the

Table I. Comparison between Inductances (H) Calculated by Three Methods

Freq (Hz)	Traditional Solver	Proposed method with inexact zero eigenvalues	Proposed method with inexact zero eigenvalues corrected
50×10^{9}	1.1452e-012	1.1452e-012	1.1452e-012
30×10^{9}	1.1452e-012	1.1452e-012	1.1452e-012
10^{9}	1.1452e-012	1.1452e-012	1.1452e-012
10^{8}	1.1453e-012	1.1357e-012	1.1452e-012
10^{7}	1.1078e-012	1.9902e-012	1.1452e-012
10^{6}	-7.1783e-012	-1.7473e-010	1.1452e-012
10^{5}	1.9878e-010	5.1647e-010	1.1452e-012
10^{4}	-1.8377e-007	5.7346e-007	1.1452e-012
10^{3}	-1.1309e-006	-2.6692e-005	1.1452e-012
10^{2}	-0.0017	-0.0107	1.1452e-012
10^{1}	0.0109	-0.4428	1.1452e-012
1	3.4740	-51.9957	1.1452e-012
10^{-16}	2.3468e+032	-7.3231e+033	1.1452e-012
10^{-32}	2.3487e+063	1.3046e+066	1.1452e-012
0	NA	NA	1.1452e-012

EFIE solution. In that case, the fast $O(1)$ solution proposed in this section that has a single vector can be extended to include a few other vectors representing the contribution from higher-order eigenmodes to obtain the solution of EFIE at all breakdown frequencies. Interestingly, when this happens, static and quasi-static approximations are even theoretically wrong at breakdown frequencies since higher-order eigenmodes with nonzero eigenvalues do not satisfy static or quasi-static physics. In addition, it is also worth mentioning that the $O(1)$ space W_0 found in this section is frequency independent, not only can it be used for frequency-domain analysis, but also for time-domain analysis.

For the plane-wave incidence case in which right hand side V is frequency dependent, at low frequencies, the EFIE solution has both real and imaginary parts. From (34), it can be seen that the real part is associated with the divergence-free current. It is a constant. As for the imaginary part, it scales with frequency linearly as can be seen from (35). Based on such a frequency dependence of the EFIE solution at low frequencies, by using a single solution obtained at ω_{ref}, we can obtain the solution of EFIE at any low frequency where the original numerical solution breaks down.

V. NUMERICAL RESULTS

The accuracy and efficiency of the proposed method have been validated by a number of circuit and scattering examples. We give three examples in the following.

A. Ring inductor

The first example is a ring inductor, the geometry of which is shown in Fig. 1, where L is 1 μm, and W is 0.25 μm. A delta-gap voltage source is applied across one edge of the triangular element based discretization of the inductor. For this example, the traditional RWG-based EFIE solver breaks down in the range of 10^{7}–10^{8} Hz. With the proposed method, we are able to extract a correct inductance at any low frequency, which agrees very well with the analytical result 1.1314 pH, as can be seen from Table I. Three methods are compared in Table I from DC to 50 GHz: the proposed method, the proposed method without correcting the inaccurate zero eigenvalues, and the traditional RWG-based MoM solution of EFIE. Clearly, the proposed method produces a correct inductance, whereas the traditional method and the proposed method with inexact zero eigenvalues both fail at low frequencies. For this example, the inductance is shown to be a constant across the whole range from zero to 50 GHz because of the small physical dimension of the structure. At 50 GHz, the electric size is 1.7×10^{-4} wavelengths; while at 10^{-32} Hz, the electric size is 3.3×10^{-47} wavelengths.

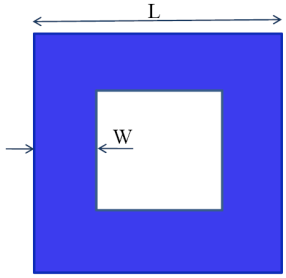

Fig. 1. Geometry of a ring inductor.

In addtion, for this example, we list the first 12 eigenvalues of (8) computed at 10^{-16} Hz in Table II. The first eigenvalue in Table II appears to be a very large number, however, it is, in fact, zero because there exists a greater than 16 orders of magnitude difference between the first eigenvalue (smallest one) and the largest one, which is

Table II. First Twelve Eigenvalues of the Ring Inductor at 10^{-16} Hz.

1	-132110042718041 - 7.73653031589450e-15i
2	3.14587874014470e+29 + 0.170125342936726i
3	3.24188695966215e+29 + 0.169696888888679i
4	1.17671618755488e+30 + 9.03492491428463e-07i
5	1.71990016645784e+30 + 3.07315770249286e-05i
6	2.67711605533504e+30 + 0.0798359149738512i
7	2.76547929854906e+30 + 0.0748445381494912i
8	3.47418985563967e+30 + 7.30378110123944e-05i
9	5.59809197867611e+30 + 3.92255723516953e-05i
10	5.83729155577273e+30 + 0.290437040167771i
11	5.94714645222034e+30 + 0.255254753252596i
12	6.52518773032250e+30 + 0.000567275418414241i

Table III. Comparison between Capacitances (F) Calculated by Three Methods

Frequency (Hz)	1e+5	1e+4	1e+3	1e+2	1e+1	1	1e-16	1e-32
C (Traditional)	4.04e-13	4.01e-13	1.29e-13	1.58e-16	-1.66e-17	5.02e-21	-4.19e-52	-2.48e-83
C (Proposed)	4.04e-13	4.04e-13	4.04e-13	4.04e-13	4.04e-13	4.04e-13	4.04e-13	4.04e-13
C (Proposed Fast)	4.04e-13	4.04e-13	4.04e-13	4.04e-13	4.04e-13	4.04e-13	4.04e-13	4.04e-13

1.4191e+31+0.02325i (not shown in the table) for this example. In double precision computing, any eigenvalue that is sixteen orders of magnitude smaller than the largest cannot be computed correctly. When this inexact zero is involved in the computation at low frequencies, the frequency dependence of the EFIE solution computed is completely wrong, which is evidient from the third column in Table I. From Table II, it can also be seen that there is a clear gap between nonzero eigenvalues corresponding to higher-order eigenmodes and the zero eigenvalue. The large gap for this example is due to the fact that the structure being simulated is small, and hence the first nonzero eigenvalue is high. In fact, as long as the structure being simulated is finite, there exists a gap between the first nonzero eigenvalue and the zero eigenvalue.

B. Parallel plate capacitor

Next, a parallel plate capacitor structure is simulated. The waveguide width, height, and length are set to be 5 mm, 4 mm, and 0.5 mm, respectively. A current source of 1 A is injected from the bottom plane to the top plane. The simulation based on a conventional RWG-based EFIE solver breaks down at 1 KHz, whereas the proposed solution is valid at all frequencies. In Fig. 3, we compare the capacitance simulated using the proposed method and that simulated by a conventional EFIE solver from 10^{-32} Hz to 1 GHz. It is clear that the proposed solution is correct at both high and low frequencies, whereas the conventional EFIE solution is wrong at low frequencies.

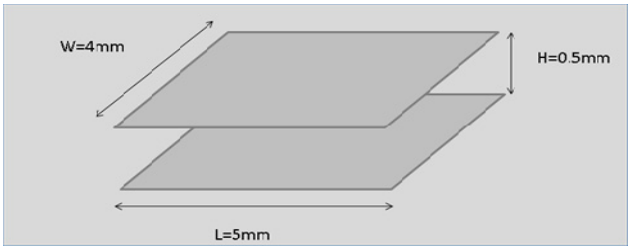

Fig. 2. Geometry of a parallel plate capacitor.

We also simulated this example by the proposed fast $O(1)$ solution described in Section IV. In Table III, we list the capacitances extracted by the conventional EFIE solution, the proposed rigorous solution shown in (26), and the proposed fast $O(1)$ solution shown in (47). It is clear that the proposed $O(1)$ solution is accurate. The relative error is less than 10^{-7} across all frequencies. The $\omega_{ref}/(2\pi)$ used in the proposed $O(1)$ solution is 100 MHz. As a result, when simulating this example from 10^{-32} Hz to 1 GHz, the solution of EFIE at all the breakdown frequencies is obtained in $O(1)$ complexity from (47).

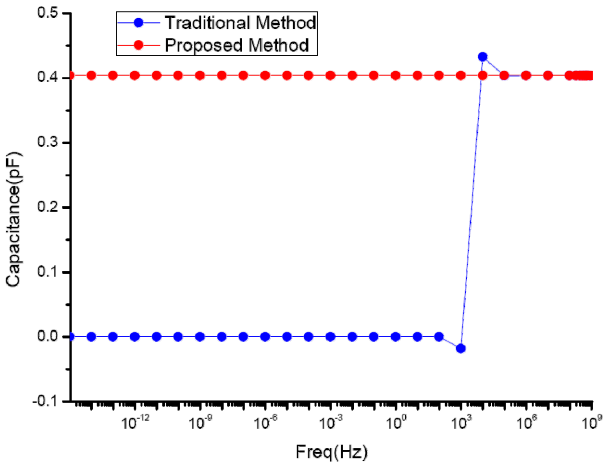

Fig. 3. Comparison of capacitances computed by the proposed method and the traditional method from 10^{-32} Hz to 1 GHz.

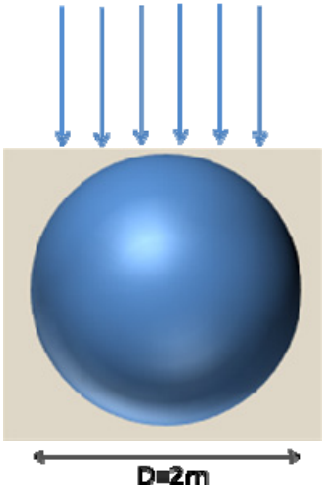

Fig. 4. A PEC sphere illuminated by a plane wave.

C. Scattering from a conducting sphere

The last example is a PEC sphere with a radius of 1 m and illuminated by a plane wave as shown in Fig. 4. We compared the far-field RCS generated by the proposed method, the traditional RWG-based EFIE method, and MIE Series at 1 Hz in Fig. 5 (a). Clearly, the result from the proposed method shows an excellent agreement with the result produced by MIE series, whereas the traditional method obviously breaks down. In Fig. 5(b), we compare the RCS generated by the proposed method, the conventional method, and that from MIE Series at a high frequency 100 MHz, where the conventional method does not break down. It is clear that the proposed method correlates very well with the conventional method and the MIE Series solution, which

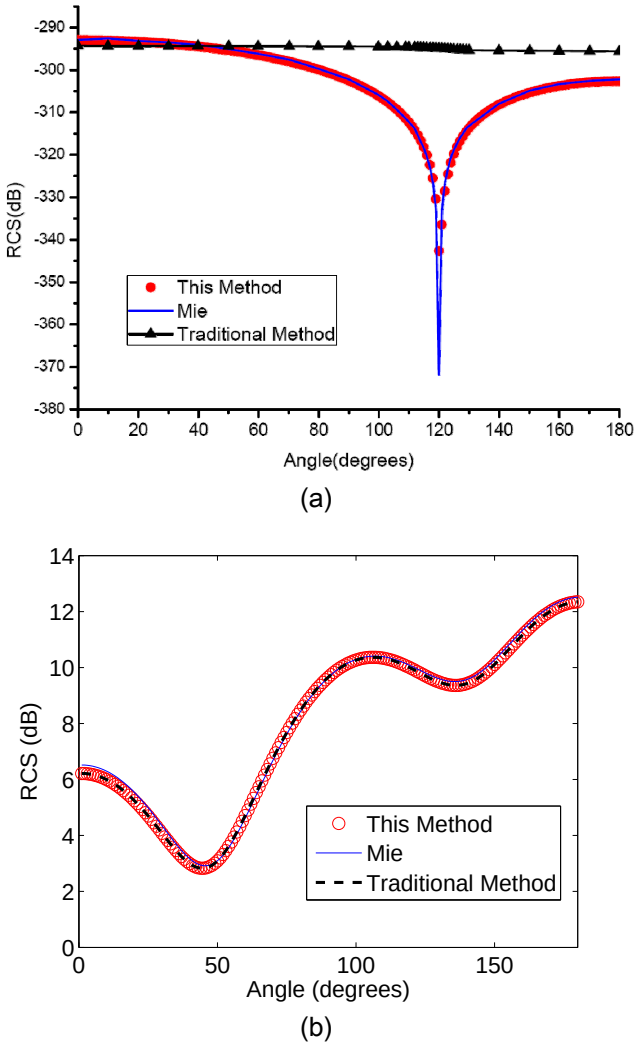

Fig. 5. The Bi-static RCS comparision. (a) 1 Hz. (b) 100 MHz.

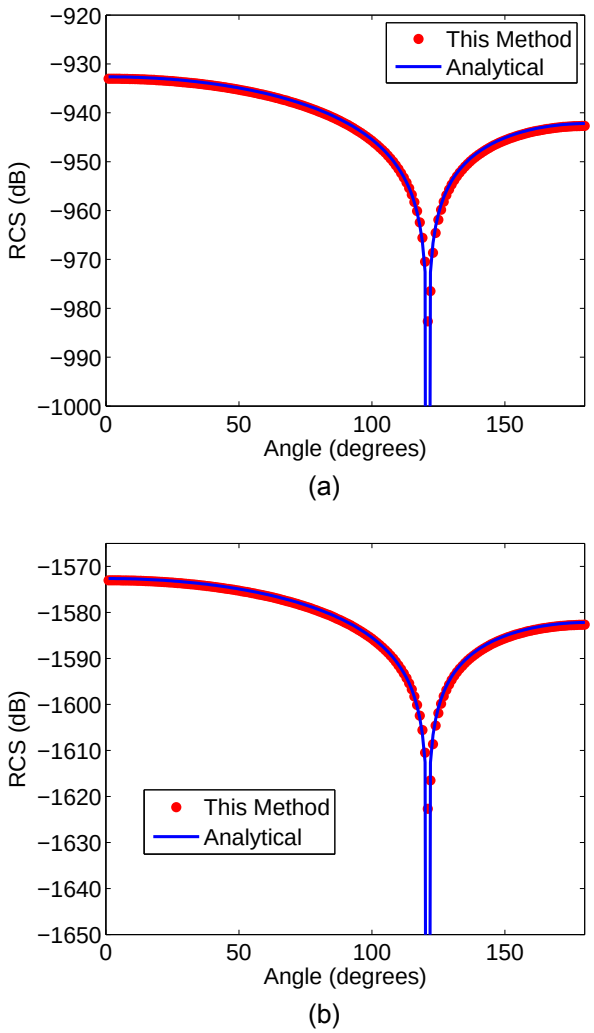

Fig. 6. The Bi-static RCS comparision. (a) 10^{-16} Hz. (b) 10^{-32} Hz.

demonstrates the fact that the proposed method is valid at both high and low frequencies.

In Fig. 6 (a) and (b) we show the RCS at 10^{-16} and 10^{-32} Hz generated by the proposed method in comparison with that obtained from analytical data [16]. Excellent agreement is observed between the proposed method and analytical solution. The analytical solution has a null at 120 degrees, which is well captured by the proposed method. In addition, it can be seen that at such low frequencies, the RCS decreases when frequency decreases, and also decreases with frequency as ω^4. In Fig. 7 (a) and (b), we compare the RCS result obtained by the proposed fast solution described in Section IV with analytical data and the result of the proposed method without the fast solution at 1 Hz and 10^{-32} Hz respectively. The accuracy of the proposed fast solution is clearly demonstrated.

VI. CONCLUSIONS

In this paper, the solution to the original RWG-based EFIE is rigorously found at arbitrarily low frequencies including DC. It does not make use of low-frequency approximations, and is equally valid at high frequencies. A fast $O(1)$ method is also developed to speed up the low-frequency computation instead of introducing additional computational cost to fix the low-frequency breakdown of EFIE. In addition, we have detailed three breakdown phenomena one can encounter in the EFIE-based low-frequency analysis, and we show how each of them is rigorously solved in this work.

The proposed solution can be employed to develop a theoretical understanding on how the solution of the EFIE should scale with frequency at low frequencies; at which frequency full-wave effects become important; given a problem, whether there exist a range of frequencies in which traditional full-wave EFIE solution breaks down while static or quasi-static approximations are not valid yet, etc. It can also shed the light on other unsolved research problems, the root cause of which is finite machine precision.

REFERENCES

[1] J. Zhao and W. C. Chew, "Integral equation solution of Maxwell's equations from zero frequency to microwave frequencies," *IEEE Trans. Antennas Propag.*, vol. 48, no. 10, pp. 1635-1645, Oct. 2000.

[2] Z. Qian and W.Chew, "Enhanced A-EFIE With Pertubation Method," *IEEE Trans. Antennas Propag.*, vol. 58, pp. 362-372, Feb. 2004.

[3] M. Taskinen and P. Yla-Oijala, "Current and charge integral equation formulation," *IEEE Trans Antennas Propag,* vol. 54, pp. 58-67, 2006.

[4] Z. Qian and W. Chew, "Fast Full-Wave Surface Integral Equation Solver for Multiscale Structure Modeling," *IEEE Trans. Antennas Propag.*, vol. 57, no. 11, pp. 3594-3602, Nov. 2009.

[5] R. J. Adams, "Physical Properties of a stabilized electric field integral equation," *IEEE Trans. Antennas Propag*., vol. 52, no. 10, pp. 3256-3264, October. 2010.

[6] F. P. Andriulli, K. Cools, H. Bagci, F. Olyslager, A. Buffa, S. Christiansen, and E. Michielssen, "A multiplicative Calderón preconditioner for the electric field integral equation," *IEEE Trans. Antennas Propag.*, vol. 56, pp. 2398–2412, Aug. 2008.

[7] Matthew B. Stephanson and Jin-Fa Lee, "Preconditioned Electric Field Integral Equation Using Calderon Identities and Dual Loop/Star Basis Functions," *IEEE Trans. Antennas Propag*., vol. 57, no. 4, pp. 1274-1278, April. 2009.

[8] S. Yan, J.-M. Jin, and Z. Nie, "EFIE Analysis of Low-Frequency Problems with Loop-Star Decomposition and Calderón Multiplicative Preconditioner," *IEEE Trans. Antennas Propag*., vol. 58, no. 3, pp. 857-867, Mar. 2010.

[9] J. Zhu and D. Jiao, "A Theoretically Rigorous Full-Wave Finite-Element-Based Solution of Maxwell's Equations from DC to High Frequencies," *IEEE Trans. Advanced Packaging*, vol. 33, no. 4, pp. 1043-1050, 2010.

[10] J. Zhu and D. Jiao, "A Rigorous Solution to the Low-Frequency Breakdown in Full-Wave Finite-Element-Based Analysis of General Problems Involving Inhomogeneous Lossless/Lossy Dielectrics and Non-ideal Conductors," *IEEE Trans. MTT*, vol. 59, no. 12, pp. 3294-3306, Dec. 2011.

[11] E. Arvas, R. F. Harrington, and J. R. Mautz, "Radiation and scattering from electrically small conducting bodies of arbitrary shape," *IEEE Trans. Antennas Propagat.*, vol. 34, pp. 66-77, Jan. 1986.

[12] J. S. Zhao, W. C. Chew, T. J. Cui, and Y. H. Zhang, "Cancellations of surface loop basis functions," *in Proc. IEEE Antennas Propag. Symp*., 2002, pp. 58–61.

[13] S. M. Rao, D. R. Wilton, and A. W. Glisson, "Electromagnetic scattering by surfaces of arbitrary shape," *IEEE Trans. Antennas Propag*., vol. 30, pp. 409–418, May 1982.

[14] G. Strang, " Linear Algebra and its Applications," Ed. 4, 2005.

[15] G. W. Stewart , "Matrix Algorithms, Volume II: Eigensystems," pp. 231-240, 2001.

[16] R. F. Hanington, "Time Harmonic Electromagnetic Fields," New York: McGraw-Hill, 1961.

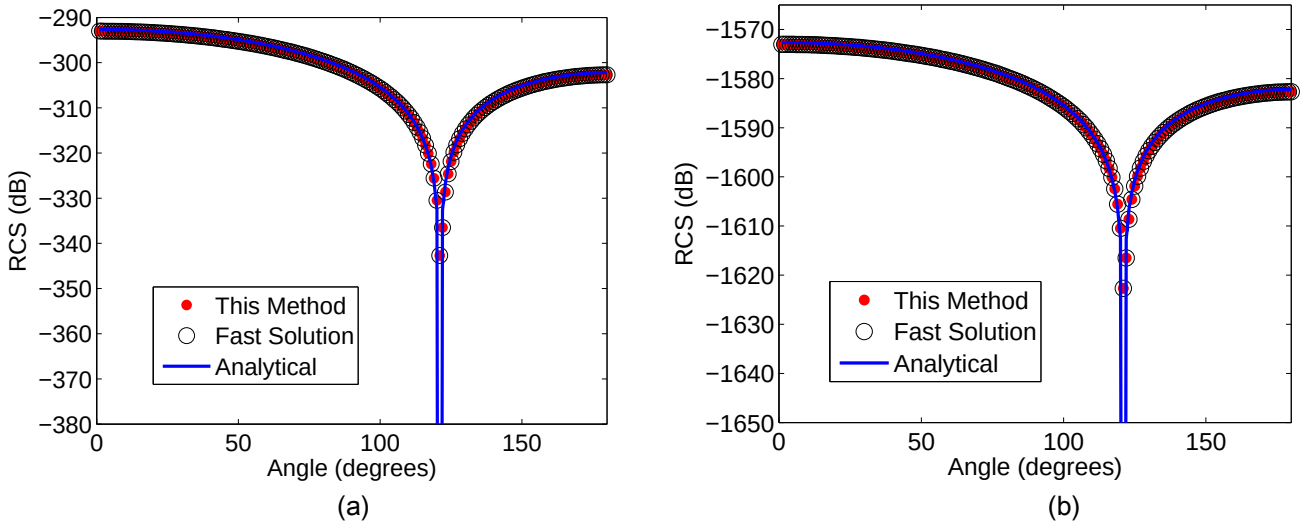

Fig. 7. Comparison between the analytical Bi-static RCS, the RCS computed by the proposed method without a fast solution, and the RCS computed by the proposed fast solution at two frequencies. (a) 1 Hz. (b) 10^{-32} Hz.